



**HAL**  
open science

## Impact of wind-driven circulation on contaminant dispersion in a semi-enclosed bay

Camille Mazoyer, Heleen Vanneste, Christiane Dufresne, Yann Ourmieres,  
Marcello Magaldi, A. Molcard

► **To cite this version:**

Camille Mazoyer, Heleen Vanneste, Christiane Dufresne, Yann Ourmieres, Marcello Magaldi, et al..  
Impact of wind-driven circulation on contaminant dispersion in a semi-enclosed bay. Estuarine, Coastal  
and Shelf Science, 2020, 233, pp.106529. 10.1016/j.ecss.2019.106529 . hal-02968335

**HAL Id: hal-02968335**

**<https://hal.science/hal-02968335>**

Submitted on 21 Jul 2022

**HAL** is a multi-disciplinary open access archive for the deposit and dissemination of scientific research documents, whether they are published or not. The documents may come from teaching and research institutions in France or abroad, or from public or private research centers.

L'archive ouverte pluridisciplinaire **HAL**, est destinée au dépôt et à la diffusion de documents scientifiques de niveau recherche, publiés ou non, émanant des établissements d'enseignement et de recherche français ou étrangers, des laboratoires publics ou privés.



Distributed under a Creative Commons Attribution - NonCommercial 4.0 International License

# Impact of wind-driven circulation on contaminant dispersion in a semi-enclosed bay

Camille Mazoyer<sup>a,b,\*</sup>, Heleen Vanneste<sup>a</sup>, Christiane Dufresne<sup>c</sup>, Yann Ourmieres<sup>a</sup>, Marcello G. Magaldi<sup>d,e</sup>, Anne Molcard<sup>a</sup>

<sup>a</sup>*Univ Toulon, Aix Marseille Univ., CNRS/INSU, IRD, MIO UM 110, Mediterranean Institute of Oceanography, La Garde, France*

<sup>b</sup>*Université de Toulon, IMATH, EA 2134, Avenue de l'Université, 83957 La Garde, France*

<sup>c</sup>*Institut des sciences de la mer, Université du Québec à Rimouski, 310 allée des Ursulines, C.P. 3300, Rimouski, Québec, G5L 3A1, Canada*

<sup>d</sup>*Istituto di Scienze Marine, S.S. di La Spezia, Consiglio Nazionale delle Ricerche, Forte Santa Teresa, Pozzuolo di Lerici (SP), I-19032, Italy*

<sup>e</sup>*Department of Earth and Planetary Sciences, The Johns Hopkins University, Olin Hall, 34th and North Charles Streets, Baltimore, MD 21218, USA*

---

## Abstract

Mediterranean semi-enclosed bays are often exposed to high levels of contaminants originating from anthropogenic activities in the bay. To assess their fate and impact on the environment, it is essential to investigate coastal circulation regimes which may play an important role in the dispersion of contaminants across the bay and beyond. In this study, a high resolution coupled hydrodynamic - passive tracer model was combined with ADCP observations, to identify major circulation patterns and associated dissolved contaminant dispersion pathways in the contaminated semi-enclosed bay of Toulon (South of France, NW Mediterranean Sea). Two dominant circulation patterns and two derived ones could be identified, driven by winds (Mistral

---

\*Corresponding author

Email address: [camille.mazoyer@mio.osupytheas.fr](mailto:camille.mazoyer@mio.osupytheas.fr) (Camille Mazoyer)

and easterly winds) and offshore waters intrusions. Medium to strong Mistral events (superior to  $6 \text{ m s}^{-1}$ ) with a WNW direction cause a bi-layer pattern with surface waters flowing out of the bay and marine waters entering at depth. Less frequently, Western Mistral winds of medium to strong strength (superior to  $6 \text{ m s}^{-1}$ ) may generate an anticyclonic circulation. During easterly wind conditions ( $> 6 \text{ m s}^{-1}$ ), an inward flow can be observed which is sometimes reinforced by offshore waters intrusions, probably from the local boundary current, the Northern Current (NC). Furthermore, dissolved contaminant dispersion pathways were simulated under typical wind forcing conditions with three source points of copper (Cu) that were identified based on surface Cu observations. While most of the WNW Mistral wind events transport dissolved copper plumes across and out of the bay, contaminant dispersion can remain confined to the bay under certain west mistral conditions. Conversely, during easterly wind events, contaminants are exiting the bay as a narrow vein along the Saint-Mandrier peninsula, before probably converging on the NC offshore. Accordingly, this study demonstrates the important impact of hydrodynamic-driven processes on the dispersion of contaminants within a semi-enclosed bay.

*Keywords:* Semi-enclosed bay, wind-driven circulation, contaminant dispersion, MITgcm, Toulon Bay

---

## 1. Introduction

Today, marine coastal areas suffer from an extremely high anthropogenic pressure, which is the result of a continuous development of human activities in these areas for centuries. These activities have lead to pollution hot

spots, endangering the water quality of ports, beaches, aquaculture zones and marine protected areas, challenging local governments to find a balance between economical and environmental interests. To this end, Toulon Bay (South of France, NW Mediterranean Sea) is an area of interest as it is a semi-enclosed bay harbouring the largest French naval base while located at less than 20 km from the Marine National Park of Port-Cros (Fig. 1). The core of this marine protected area includes two islands within the Hyeres Bay, namely Porquerolles and Port-Cros Islands. The surrounding waters, hosting a unique marine ecosystem, are highly monitored to maintain its quality, protect its biodiversity and promote a sustainable development of tourism and local communities. Its proximity to the highly industrialised Toulon city requires a better understanding of contaminant distribution within the bay and its surroundings, to assess its potential impact on the water quality of the national park. The long history of naval, industrial and commercial activities in the Toulon Bay has important environmental consequences for the bay. High concentrations of trace metals (e.g. lead, copper, zinc, ...) have been measured in sediments (Tessier et al., 2011; Pougnet et al., 2014) and surface waters (Dang et al., 2015; Jean et al., 2012; Coclet et al., 2018). For both matrices, the contamination is the strongest in the enclosed north-western part of the bay (i.e. the small Bay (SB)) where surface sediments contain up to ca. 1000 times more mercury compared to background values, while up to 80, 40 and 31 times more copper, zinc and lead, respectively (Tessier et al., 2011). Surface waters on the other hand, are ca. 40 and 70-fold enriched in respectively dissolved lead and copper (Coclet et al., 2018), compared to trace metal concentrations observed in the open Mediterranean Sea (Tovar-

[Sanchez et al., 2014](#)). While Toulon Bay might be considered as one of the most polluted marine areas of the northern Mediterranean sea ([Tessier et al., 2011](#)), contamination might be exported to offshore waters through hydrodynamic processes and reach sensitive areas as the Marine National Park of Port-Cros.

Very few studies have focused on the hydrodynamic processes within the Toulon Bay. [Millot et al. \(1981\)](#) and [Tine \(1981\)](#) were the first to use current profiler data to quantify water exchanges through the channel between the small (SB) and the large bay (LB), while [Duffa et al. \(2011\)](#), [Dufresne et al. \(2014\)](#) and [Dufresne et al. \(2018\)](#) recently constructed a hydro-sedimentary model of the Toulon Bay, to create a post-accidental management tool in the event of radionuclide releases to the environment. These studies showed that the circulation is strongly dependent on wind conditions, causing for instance reversals in the water column in the channel connecting the SB with the LB ([Dufresne et al., 2014](#)). While these studies focused on the quantification of the exchanges between the SB and the LB, here we investigate the circulation in the LB under various wind conditions and the resulting exchanges with offshore waters.

The aim of this study is two-fold. The first objective is to identify dominant circulation patterns inside the bay, using an ocean circulation model (MITgcm) and ADCP observations in the Toulon Bay. The second objective is to investigate contaminant transport, by defining dispersion patterns and assess the potential impact on key areas within the bay and beyond.

After a description of the studied site, the model configuration and in situ observations, we describe the wind-driven circulation within the bay.

An analysis of the contaminant distribution as observed in March 2017 is discussed and the model is used as a tool to simulate the dispersion of dissolved contaminants based on wind conditions.

## 2. Material and methods

### 2.1. Study area

The water circulation of the southeast French Mediterranean coast, is characterized by a strong geostrophic boundary current flowing along the North Western Mediterranean Sea coast counter-clockwise, the Northern Current (NC). This current has been largely studied especially focusing on its behaviour upstream in the Ligurian basin ([Taupier-Letage and Millot, 1986](#); [Alberola et al., 1995a](#); [Sammari et al., 1995](#); [Bethoux et al., 1982](#)), downstream at the eastern side of the Gulf of Lion ([Alberola and Millot, 2003](#); [Conan and Millot, 1995](#); [Flexas et al., 2002](#)), and along its shelf ([Auclair et al., 2001](#); [Petrenko, 2003](#); [Rubio et al., 2009](#); [Lapouyade and Durrieu de madron, 2001](#)). However few studies on the NC circulation were conducted in the Var region, which can be seen as an area of transition ([Ourmières et al., 2011](#); [Guihou et al., 2013](#); [Declerck et al., 2016](#)). These studies showed that in this area the NC has a meso and sub-mesoscale activity which can create exchanges between the shelves and offshore waters. For instance [Declerck et al. \(2016\)](#) modelled intrusions into the Hyeres Bay, nearby the Toulon Bay. They showed that the NC, through meanders and vortices dynamics, can either act as a barrier or favour in- and off-shore water mixing into semi-enclosed bays as Hyeres Bay. Here, we will focus on the Toulon bay, analyze its inner wind-driven circulation and the possible offshore waters intrusions

that may be driven by the Northern Current that flows off the bay.

Toulon Bay is a shallow semi-closed area (about 10 km x 15 km), divided into two bays, separated by a seawall of 1.4 km long modeled impervious on the whole water column: a small bay (SB;  $\approx 10 \text{ km}^2$ ) which hosts mostly all the anthropogenic activities and a large bay (LB;  $\approx 42 \text{ km}^2$ ) connected to the offshore sea (Fig. 1). The LB is delimited by Cape Carqueiranne to the east, and by the Saint-Mandrier peninsula to the west. At the south of the LB, the bathymetry is very steep with a canyon of ca. 600 m deep.

Since there is no significant tide motion (tidal amplitude of approximately 20 cm) (Millot et al., 1981; Alberola et al., 1995b) in the Toulon bay, its circulation is supposed to be mostly wind-driven with possible boundary current intrusions. The wind forcing has an important spatial and temporal variability with strong events (Millot et al., 1981; Dufresne et al., 2014). Three wind situations can be distinguished: Mistral, easterly wind and calm weather. Toulon is surrounded by mountains that deflect these winds: the Mistral blows from the west/north-west, especially in winter and spring. It is a cold, dry and strong wind unlike the easterly wind (from north-east to south-east) that usually brings clouds, rain and waves.

## *2.2. Model description*

The M.I.T General Circulation Model (MITgcm) is a primitive equation ocean circulation model (Marshall et al., 1997). It is a z-coordinate finite-volume model that solves the incompressible Navier-Stokes equations under Boussinesq approximation, on an Arakawa-C grid. In this model, the free surface equation is based on a pressure correction method. For this study, we use the hydrostatic approximation. The time scheme is a quasi second

order Adams Bashford and the horizontal advection scheme is the third-order DST (direct spacetime) flux limiter. The horizontal subgrid-scale mixing is parametrised with the biharmonic Leith viscosity (see [Leith, 1968, 1996](#)). Vertical background viscosity is set with  $Az = 10^{-5} \text{ m}^2 \text{ s}^{-1}$ , a standard value. We use the turbulent closure scheme K-profile parameterisation (KPP) from [Large et al. \(1994\)](#), to model vertical sub-grid scale mixing. For atmospheric forcing, we use the bulk formulation from [Large and Yeager \(2004\)](#), and open boundary conditions are prescribed and relaxed by a sponge layer. Free-slip boundary conditions are applied at the bottom and on the lateral boundaries.

### *2.3. MITgcm high-resolution configuration TBAY100*

The Toulon Bay domain spans a longitudinal range from  $5.88^\circ$  to  $6.13^\circ\text{E}$  and a latitudinal range from  $43.04^\circ$  to  $43.13^\circ\text{N}$  (Fig. 1). The horizontal mesh has 200x100 grid points with 100 m resolution. There are 75 depth levels with a 50 cm minimum layer thickness at the surface, increasing to about 30 meters near the seabed. Minimum depth is 3 meters and maximum depth is 602 meters in the canyon at the south boundary (Fig. 1). The timestep is 5 seconds. Outputs are saved every hour to catch most of the dynamics variability. The TBAY100 configuration has two open boundaries (south and west) and is forced with a NEMO-based configuration ([Declerck et al., 2016](#)) which is a 1/192 degrees configuration of the Var coast (hereafter NIDOR192), including the Hyeres Bay and the “Îles d’Or” islands (i.e. Porquerolles, Port-Cros and Levant; Fig. 1). Indeed, TBAY100 is the third level of nested coarser models (GLAZUR64, NIDOR192). GLAZUR64 and NIDOR192 have been validated during previous studies ([Ourmières et al., 2011](#); [Guihou et al., 2013](#)). The rigorous downscaling set-up guarantees good

confidence in the last and highest resolution configuration TBAY100. The horizontal velocities and mass fields open boundary conditions are uploaded daily. The operational global model ARPEGE from Meteo-France is used as atmospheric forcing: it has a 1/10 degrees spatial resolution (about 9.5 km at our latitude) and a 3 hours temporal resolution.

The starting date is the 1st of February 2016, after a 1 month simulation (spin-up evaluated to 15 days). Initial conditions are computed from NIDOR192 output.

#### *2.4. MITgcm ptracers package*

We used in this study the *ptracers* package from the MITgcm model. This is a passive tracer package, in which the dissolved tracers do not affect actively the physics of the ocean as they do not affect the water density. Tracers are initialized with precise quantities (for details see Section 4), and are released every time step.

#### *2.5. ADCP*

Horizontal velocity data from Acoustic Doppler Current Profilers (ADCP, 600 kHz, RDInstruments) were also used. Sampling frequency was 10 min. Two ADCPs were moored in the south of the LB between January 2012 and April 2012 (see Fig. 1B ). Their location were chosen to measure the exchanges between the LB and offshore. ADCP 1 was located near Cape Cepet and ADCP 2 was located near Cape Carqueiranne. The ADCPs were bottom-moored at 32 m, and 29 m respectively. The water column was divided into 35 1m-thick bins with the first bin at 2 m above the bottom.

## 2.6. Diagnostics - composites pictures

Previous studies on the area (Milot et al., 1981; Dufresne et al., 2014) concluded that atmospheric forcings strongly influence hydrodynamics into the Toulon Bay. Strong weather conditions cause highly variable currents (due to various processes such as offshore swell, wind gusts,... ) combined with offshore waters intrusions and temporal reversals. The wind rose depicted in (Fig. 2) is computed from the Meteo-France ARPEGE model dataset used as external atmospheric forcings for the oceanic model (TBAY100). Two major wind regimes can be defined accordingly:

1. A medium to strong Mistral (258.75 degrees to 326.25 degrees): a west to north-west wind with an intensity between 6 and 24 m s<sup>-1</sup> (24.9 % of the time);
2. A medium to strong easterly wind (56.25 degrees to 101.25 degrees): a south-east to a north-east wind with an intensity between 6 and 24 m s<sup>-1</sup> (9 % of the time);

When the wind intensity is lower than 6 m s<sup>-1</sup>, we consider to be under calm conditions (i.e. no wind). The circulation within the bay is therefore analyzed for each wind condition. We averaged the horizontal velocity fields associated with the specific wind regime, for the surface layer (0-5m) and across the capes section (red line on Fig. 1) defining the LB limit. These composites pictures are a powerful tool to highlight an average circulation and its variability under specific conditions.

## 2.7. Datasets

Table 1 gives an overview of all data presented, and their date ranges. As one of our main goal is to study contaminant dispersion, we have decided to simulate the year 2016-2017 to coincide with dissolved copper observations available for March 2017. Simulations are validated by a comparison with ADCP observations obtained in 2012 (see section 2.5). In order to focus on the wind-driven circulation, the velocities simulated by the model and measured by the ADCP have been filtered. Data have been processed with the PL66 filter (Limeburner et al., 1985), in order to filter all motions under 25h, including inertial oscillations, diurnal and semidiurnal tidal constituents and eigen motions.

In the next sections, we will first identify the main circulation patterns induced by regional wind characteristics and provide a quantitative validation using ADCP observations. Subsequently, results of 2 days simulations with idealized wind conditions will be presented showing the principal contaminant dispersion pathways in the Toulon Bay. These simulations benefit from the 1-month spin-up of the longer simulation TBAY100-PHYS. Eventually, the TBAY100-TRAC 14-month simulation will allow the assessment of long-term temporal variability in contaminant dispersion, by running a continuous contaminant release from 3 sources representing the main civil ports in the SB (black dots on Fig. 1B).

Table 1: The data ranges of the presented data.

Data (observations or simulations)	Dates
ADCP Cepet	January-April 2012
ADCP Carqueiranne	January-April 2012
Seawater samples	20 March 2017
Simulation TBAY100-PHYS (physics)	February 2016 - April 2017
Simulation TBAY100-TRAC (tracers)	February 2016 - March 2017
Idealized simulations	/

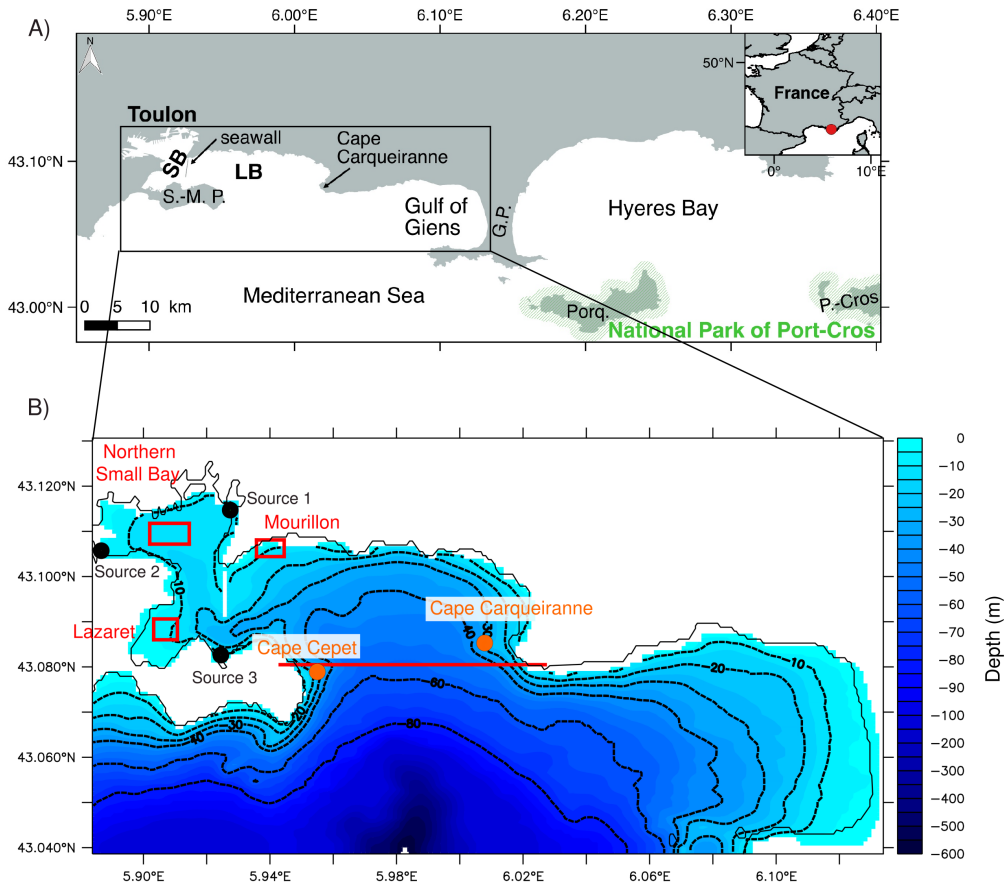


Figure 1: A) Map of Toulon Bay and its surrounding area (SB: small bay, LB: large bay, S.-M. P.: Saint-Mandrier peninsula, G. P.: Giens peninsula, Porq.:Porquerolles, P.-Cros: Port-Cros). The black box indicates the geographical extent of the model domain of TBAY100. B) Zoom of Toulon Bay with bathymetry (m). The white line between the SB and the LB indicates the impervious seawall on the whole water column. Orange dots indicate ADCP locations: Cape Cepet and Carqueiranne. The red line indicates the position of the vertical cross-section presented in Figs. 6 and 8. Black dots indicate the positions of the three contaminant sources: Toulon civil port (source 1), la Seyne-sur-Mer civil port (source 2), and Saint-Mandrier civil port (source 3). Red boxes: locations for which temporal contaminant dispersion is discussed in section 4.0.2.

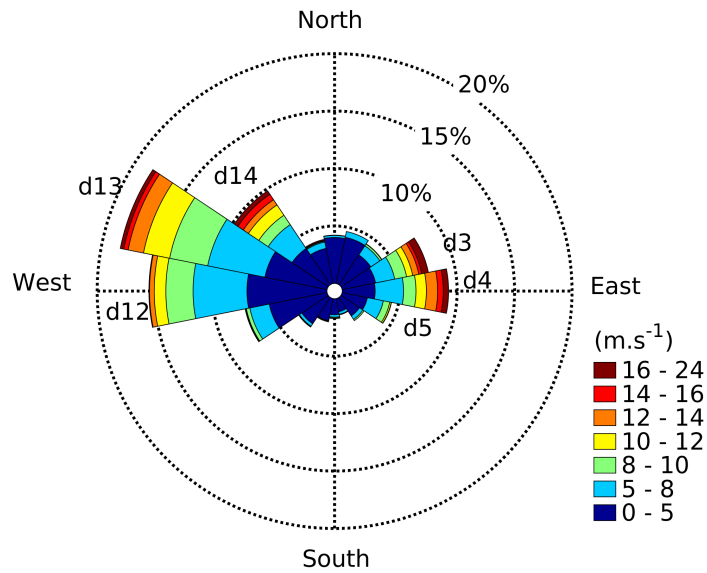


Figure 2: Windrose for winds used as external forcings from Meteo-France ARPEGE model, from February 2016 to May 2017. Directions are divided into 16 slices of 22.5 degrees each. Mistral wind is composed of west-northwest winds with three main directions: d12, d13, d14 from 258.75 degrees to 326.25 degrees. Easterly wind is composed of east-northeast winds with three main directions: d3, d4 and d5 from 56.25 degrees to 123.75 degrees. Note the windrose shows the direction from where the wind blows.

### 3. Circulation regimes

#### 3.1. Surface composite pictures

Composite pictures of surface currents (0-5m) for Mistral and easterly wind, obtained with model results, show opposite current directions induced by the two wind regimes (Fig. 3a,c). Overall, Mistral drags the surface water southeastwards (Fig. 3a) enhancing the surface current intensity near Cape Cepet and Cape Carqueiranne, whereas easterly wind pushes it towards the north-west (Fig. 3c). While Mistral events drive the surface circulation across the entire bay, the influence of easterly wind in the LB is limited (indicated by the small arrows on Fig. 3c). However in the southern part of the model domain, current intensities are higher and have a stronger gradient compared to Mistral conditions. This may be due to intrusions of offshore waters that amplify the local wind-driven current. To evaluate the relative importance of these intrusions, we computed a transport index across two transects (Fig. 3c and d), inspired from the method used by [Barrier et al. \(2016\)](#) for the quantification of intrusions in the Gulf of Lion. While T1 (Fig. 4) allows us to trace the occurrence of surface offshore waters intrusions near the southern boundary of the model domain, T2 identifies water intrusions in the LB. The northward meridional current velocity was used to calculate the positive transport  $T^+$  across each transect over the surface (2 to 10 m depth to focus on the core of the water intrusions). The transects locations were chosen where the current intensities are large combined with a standard deviation greater than  $0.1 \text{ m s}^{-1}$  for T1 and  $0.05 \text{ m s}^{-1}$  for T2 (Fig. 3c,d). The T1 transect ends westward at the canyon location which is a natural bathymetric guidance of offshore water intrusions. Transport is normalised

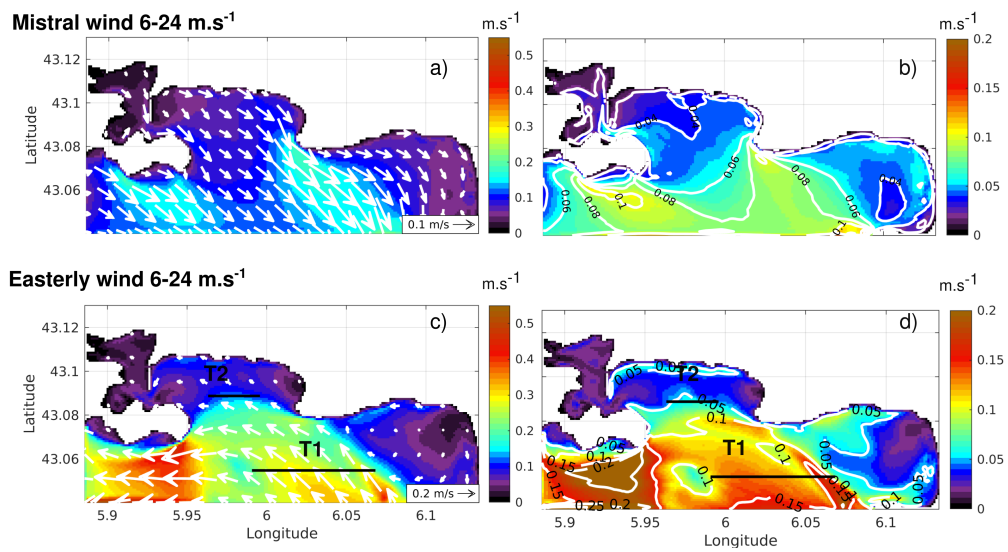


Figure 3: Left panels (a,c) are composite pictures of surface currents ( $\text{m s}^{-1}$ ). Right panels (b,d) are standard deviations of surface currents for the composite pictures ( $\text{m s}^{-1}$ ). Top panels (a,b) are for medium to strong Mistral (6 - 24  $\text{m s}^{-1}$ ), bottom panels (c,d) are for medium to strong easterly wind (6 - 24  $\text{m s}^{-1}$ ). The black lines T1,T2 are the cross-sections for the meridional transport estimations.

by its temporal mean  $\langle T^+ \rangle$ :

$$I(t) = \frac{T(t)^+}{\langle T^+ \rangle} \quad (1)$$

We consider intrusions to occur when index  $I(t) \geq 1$ , i.e. when the cross-section positive transport exceeds its mean. Fig. 4 represents the time evolution between February 2016 and April 2017 of the wind (a), T1 (b) and T2(c). As expected, most (94% ) of the easterly wind episodes (grey boxes) are associated with T1 intrusions. More than 13 periods reveal strong intrusions with a high T1 index (up to 6-7).

Hence, during medium to strong easterly wind periods, offshore surface waters are pushed toward the LB, bending in a cyclonic circulation at the bay entrance. Whether or not the offshore waters enter the bay can be evaluated by the T2 index. During three episodes (episodes 1, 2 and 6 in Fig. 4), a T2 index higher than 3 highlights the presence of an intrusion within the LB. At other times (episodes 3,4 and 5), the T2 index remains below the index value 3, indicating that the current mainly bypasses the LB. T2 intrusions have been estimated to occur in the LB 78% of the time during easterly wind episodes.

To evaluate the influence of the wind on the intrusion into the LB, a scatter plot in Fig. 5 was used to represent the T1 and T2 indexes according to the wind intensity and direction.

Very high values of T1 occur 16% of the time for E-NE strong winds (all points circled by the black line in Fig. 5) corresponding to a non intrusion circulation (T2 small), while high values of T2 (and T1 larger than 1) occur with medium (around  $8 \text{ m s}^{-1}$ ) north-easterly wind (90-120 degrees) (all points circled by the red line in Fig. 5b). The wind direction combined with

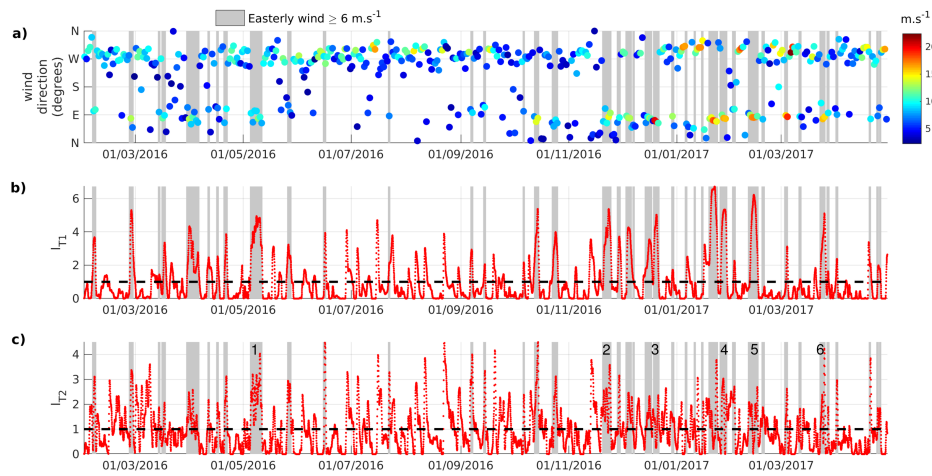


Figure 4: Model results during February 2016 - April 2017 period including (a) wind intensity ( $\text{m s}^{-1}$ ) and direction (from which the wind blew) from Meteo-France ARPEGE model; (b) index intrusion for transect T1; (c) index intrusion for transect T2. Locations of T1 and T2 transects are black lines in Fig.3. Grey boxes are medium to strong easterly wind periods. The horizontal dotted line corresponds to the detection threshold of intrusions.

its intensity seem to be the main forcings triggering intrusions of offshore water in the LB. The remaining 6% correspond to situations without intrusion near the southern boundary nor into the LB.

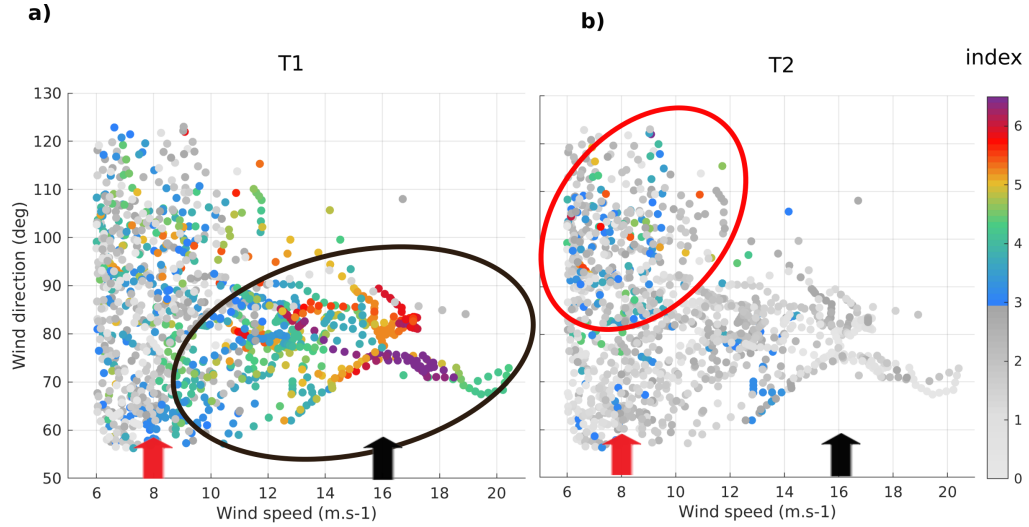


Figure 5: Scatter plot of wind speed ( $\text{m s}^{-1}$ ) versus wind direction (deg). The colorbar indicates the value of T1 index (a) or T2 index (b). Red circle corresponds to winds with an entrance in the domain and in the LB. Black circle corresponds to winds with an entrance in the domain but no entrance in the LB. Red arrow corresponds to a wind of  $8 \text{ m s}^{-1}$  and black arrow corresponds to a wind of  $16 \text{ m s}^{-1}$ .

### 3.2. Cross-section composite pictures

After having investigated surface circulation, this section aims at studying the circulation through depth. To study the impact of wind conditions on the entire water column, circulation has been studied along a vertical cross-section between Cape Cepet and Cape Carqueiranne (red line in Fig. 1B).

For a medium to strong Mistral wind ( $6\text{-}24 \text{ m s}^{-1}$ ), results show a bi-layer circulation into the bay (Fig. 6a), as it was shown for certain time periods by

Duffa et al. (2011). We clearly see here that the surface layer flows southward (blue) towards the open sea with a maximum mean value of  $0.18 \text{ m s}^{-1}$  near Cape Carqueiranne, whereas an incoming flow enters (red) the LB at the bottom of the water column (10-40 m). The average inversion depth is at ca. 10 m depth at the center of the channel, and it can deepens for strong winds.

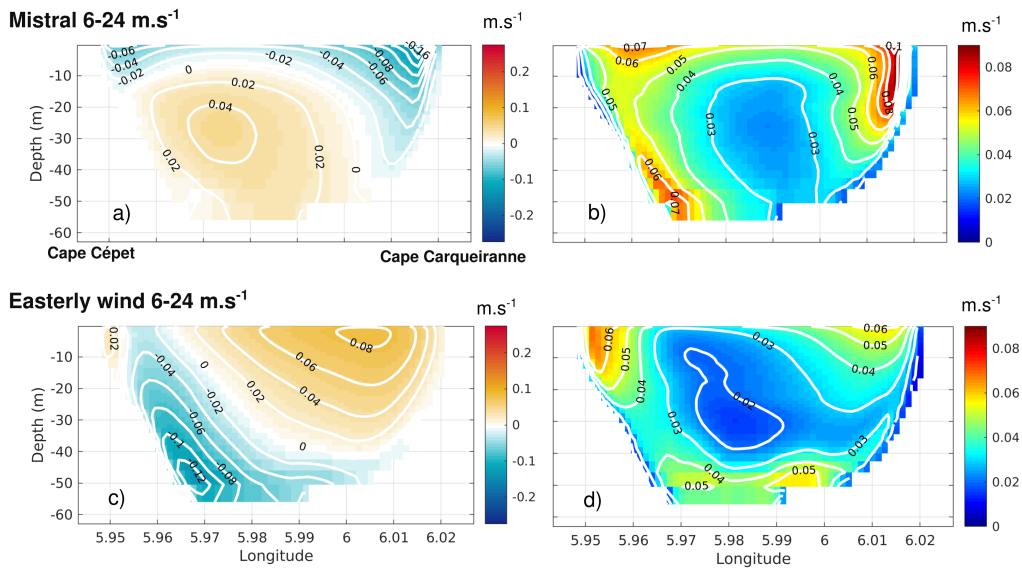


Figure 6: Left panels (a,c) are composite pictures of meridional velocity on a vertical cross-section between Cape Cépet and Cape Carqueiranne (red line in Fig. 1B). Right panels (b,d) are standard deviations of the meridional velocities for the composite pictures. Top panels (a,b) are for medium to strong intensity Mistral ( $6 - 24 \text{ m s}^{-1}$ ), bottom panels (c, d) are for medium to strong easterly wind ( $6 - 24 \text{ m s}^{-1}$ ).

In order to evaluate the occurrence of the bi-layer circulation, the meridional velocities were integrated at the surface (0-10 m) (blue box in Fig. 8a) and below the inversion depth (20-40 m) (red box in Fig. 8a) in order to avoid its variability. Results show that the bi-layer pattern, defined by a

inward surface flux, and outward deep flux, and according to our criteria, occurs for 81% of the Mistral events. The standard deviation on the outcoming current along Cape Carqueiranne (Fig. 6b) suggests that velocity variations are more important in this outflow compared to cape Cepet. A bathymetric effect is a probable explanation for this current acceleration near this cape induced by stronger wind. Overall the standard deviation of the meridional current across the vertical section has the same order of magnitude of the current itself. This can suggest that the bi-layer system may not be the only possible scheme.

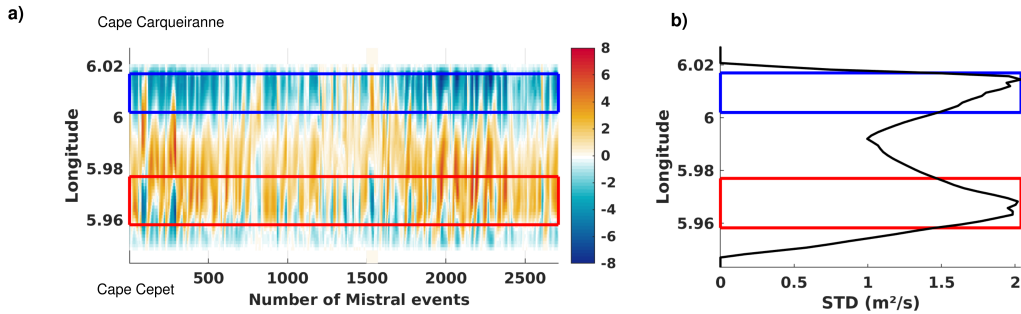


Figure 7: Left panel (a) is a depth integration of meridional velocity on a cross-section between Cape Cepet and Cape Carqueiranne (red line in Fig. 1B) through number of Mistral events ( $6 - 24 \text{ m s}^{-1}$ ). Right panel (b) is the standard deviation of the meridional velocity through time. Red and blue boxes are locations where  $\text{STD} \geq 1.5$ .

The transport across this section (Fig. 7b) for all the events corresponding to the Mistral regime is globally in the direction of the wind near the capes and upwind in the middle of the section. The same observation was first shown for an idealized long narrow lake by Csanady (1973), where the transport is downwind in shallow parts of the lake and upwind in deeper parts. This observation has also been made in the Gulf of Trieste a Mediter-

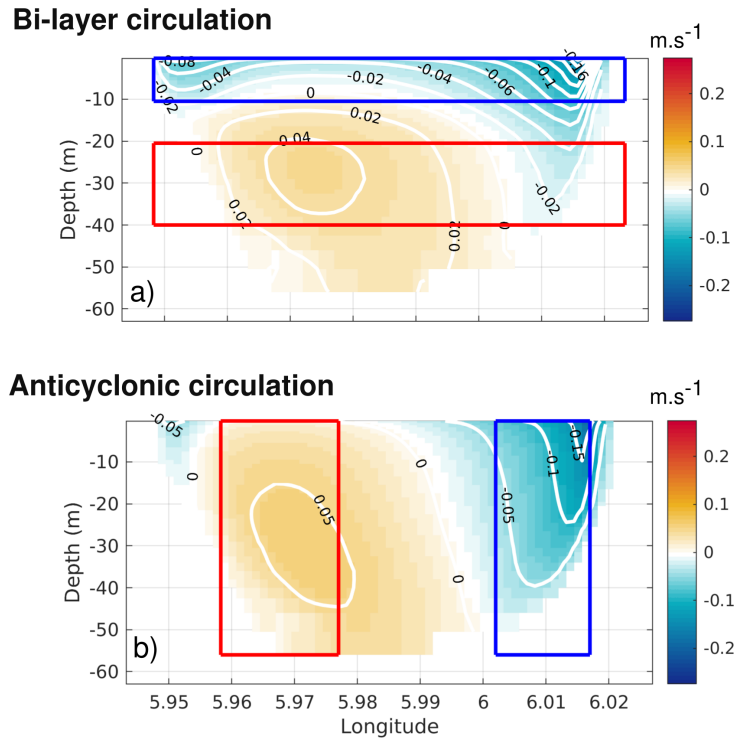


Figure 8: Composite pictures of meridional velocity on a vertical cross-section between Cape Cepet and Cape Carqueiranne (red line in Fig. 1B). Top panel (a) is for a bi-layer circulation (Mistral 6 -  $24 \text{ m s}^{-1}$ ), bottom (b) is for an anticyclonic circulation (Mistral 6 -  $24 \text{ m s}^{-1}$ ). Red and blue boxes are used for transport analysis (red for positive and blue for negative).

ranean semi-enclosed basin (Malačić et al., 2012), in coastal lagoons (Fian-drino et al., 2017) and in a shallow estuarine lake (Schoen et al., 2014) for wind-driven circulation.

The Toulon Bay bi-layer pattern typical of the classic “wind driven channel circulation” is the dominant pattern during Mistral wind conditions, occurring 81% of the Mistral-driven circulations. The composite picture resulting in this BLP is depicted in Fig. 8a. The events are selected according to the transport value in the upper/lower layers imposed negative at the surface and positive at depth (blue/red boxes in the figure).

Looking closer around the capes (boxes in Fig. 7b), the standard deviations of the integrated meridional velocity have very high values, exceeding  $1.5 \text{ m}^2 \text{ s}^{-1}$ , revealing inversions of the currents along the capes. In particular, another possible circulation pattern can result from the Mistral wind regime, when the inflow (upwind) at the western Cape Cepet emerges and fills the whole water column. By extracting the remaining events, having an inflow at the western Cape, and an outflow at the eastern Cape (Fig. 8b, red boxes), an anticyclonic circulation within the LB is revealed during 13% of the Mistral events.

Medium to strong easterly winds ( $6\text{-}24 \text{ m s}^{-1}$ ) appear to generate an inward flow into the LB on the east side (Fig. 3c), with a core positioned at the surface near Cape Carqueiranne (Fig. 6c). The outflowing current follows the bathymetry at the westside of the cross section, near Cape Cepet, with its core at ca. 50 meters depth. A small confined inward current appears to occur at the edge of the cross-section (Cape Cepet), although standard deviations (Fig. 6d) show that its behaviour is very variable. Indeed, this

current can also disappear for instance when the surface current along the entire section enters the LB (not shown). Note that a significant fraction of the surface current bypasses the LB.

The analysis of the composite pictures described above, not only corroborates the previously identified highly variable nature of the hydrodynamics in the Toulon Bay (Duffa et al., 2011; Dufresne et al., 2014), but it also clearly allows to associate circulation patterns with typical wind characteristics.

### 3.3. Main circulation patterns

A qualitative and quantitative analysis of the model results, using the composite pictures described in section 3.1 and 3.2, allows the identification of four distinct circulation patterns, depending on the wind regimes and the offshore waters intrusions:

1. The Bi-layer pattern (*BLP*; Fig. 9a): the predominant circulation pattern during medium to strong Mistral events (81%). It occurs mainly with a west-northwest wind, with a median intensity of  $8.88 \text{ m s}^{-1}$ . It is characterised by a unidirectional surface outflow to the southeast towards the open sea inducing a bottom current entering the Toulon Bay (Fig. 8a). The maximum velocities observed near Cape Carqueiranne are due to a cape effect;
2. The Anticyclonic pattern (*ACP*, a derived circulation from the BLP pattern; Fig. 9b): a barotropic inward flow near Saint-Mandrier peninsula that follows the bathymetry in an anticyclonic way and leaves the LB near Cape Carqueiranne. This circulation pattern occurs 13% of medium to strong Mistral wind events. It occurs with a west to

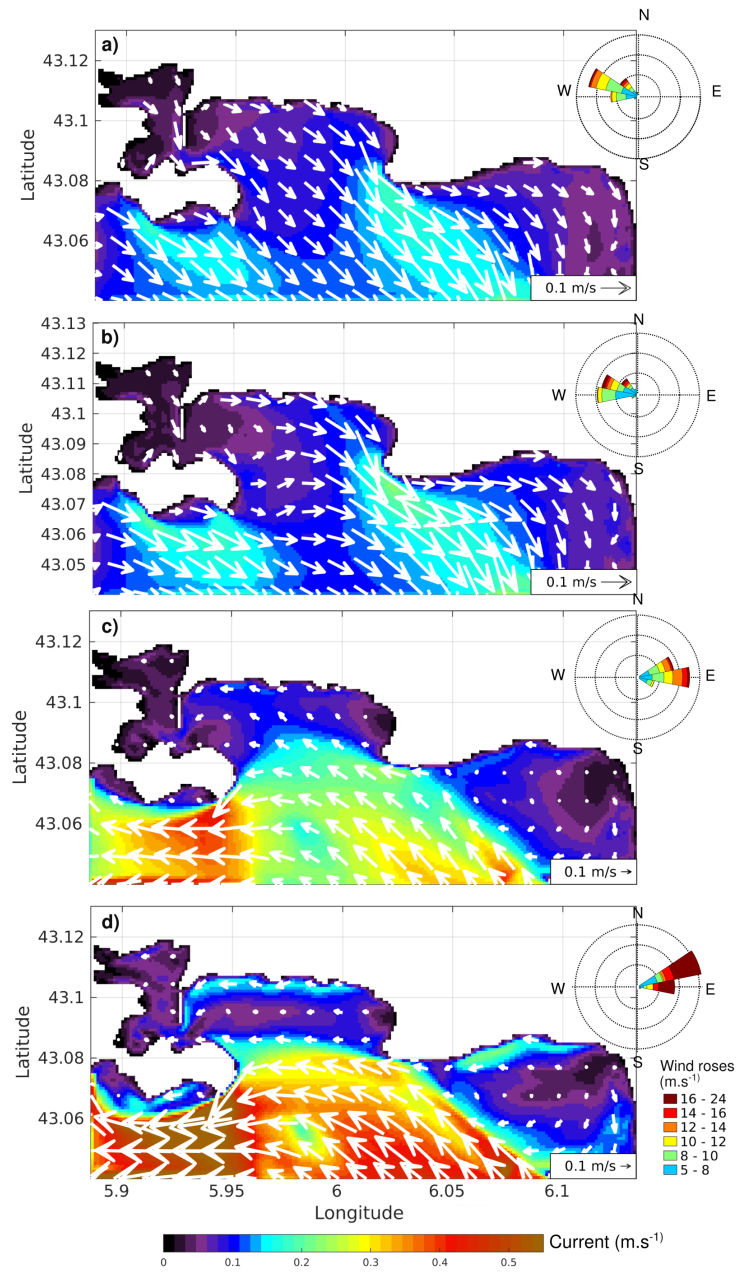


Figure 9: Composites pictures of surface velocities ( $\text{m s}^{-1}$ ) showing the 4 circulation patterns: a) BLP pattern, b) ACP pattern, c) IP pattern, d) NIP pattern. A wind rose is presented for each pattern.

west-northwest wind, with a median intensity of  $8.22 \text{ m s}^{-1}$  and mostly during winter periods meaning the absence of stratification can play a role for its occurrence. In most cases, a small confined current flows southeastwards along the Saint-Mandrier peninsula (Fig. 8b);

3. The Intrusion pattern (*IP*; Fig. 9c) : an inward flow near Cape Carqueiranne, caused by an offshore waters intrusion into the LB during easterly wind events (with median intensities of  $9.15 \text{ m s}^{-1}$ ). This pattern has been highlighted by a transport analysis to detect offshore waters intrusions into the LB. It has been identified to occur for 78% of the time when easterly winds exceed  $6 \text{ m s}^{-1}$  and for wind from 80 to 120 degrees most of the time. South of the open boundary line, this circulation pattern has a cyclonic character, probably mainly driven by the along-coast pathway of the NC. These offshore waters intrusions depend on the upstream circulation features, and more specifically on whether an NC intrusion into the Hyeres Bay has occurred (Declerck et al., 2016).
4. The Non Intrusion pattern (*NIP*; Fig. 9d) : this derived regime from the IP pattern has also an anti-clockwise circulation south of the open boundary line, induced by medium to strong easterly wind events with a predominant northeast direction (60 to 90 degrees) to with a median intensity of  $15.18 \text{ m s}^{-1}$ , which is greater than for the IP pattern. It occurs 16% of the time when easterly winds exceed  $6 \text{ m s}^{-1}$ . This pattern is characterized by strong current intensities located mainly south of the LB and by no waters intrusions in the LB.

It is worth mentioning that the criteria used to identify the four distinct

circulation patterns can be differently chosen, and may give slightly different percentage of occurrence. However, the four patterns are clearly present in the simulations, and this will be confirmed with the distribution of contaminant (section 4).

### *3.4. Validation with in-situ observations*

The Toulon Bay model TBAY100 is the third level of nested coarser models (GLAZUR, NIDOR) (see section 2.3), with accurate forcings at the southern and western boundaries. Nevertheless, validations with in-situ observations is necessary and will emphasis our confidence in the previous results. In-situ current observations in such coastal areas are scarce. ADCP data were only available from January to April 2012. The model results are compared to these ADCP observations by sorting and averaging the velocities obtained during the two typical wind conditions of the area. Surface (top 2.5 m) and bottom currents (28 m) resulting composites, computed by the model and recorded by both ADCPs at Cape Carqueiranne and Cepet, are presented in the current rose diagrams in Fig. 10 as average percentages through the ADCP deployment period and the total period of the model simulation. The figure is split in 4 boxes: left ones correspond to Cape Cepet ADCP analysis, right ones correspond to Cape Carqueiranne; upper blue boxes correspond to Mistral wind regime, and lower orange ones to easterly wind regime. In each box 4 current roses are designed for the observation, the model, the surface and the bottom.

At Cape Cepet, during medium and strong Mistral winds, (upper left box) surface modelled and observed currents flow towards the same direction, i.e. south-east (Fig. 10a and b), although modelled intensities are stronger

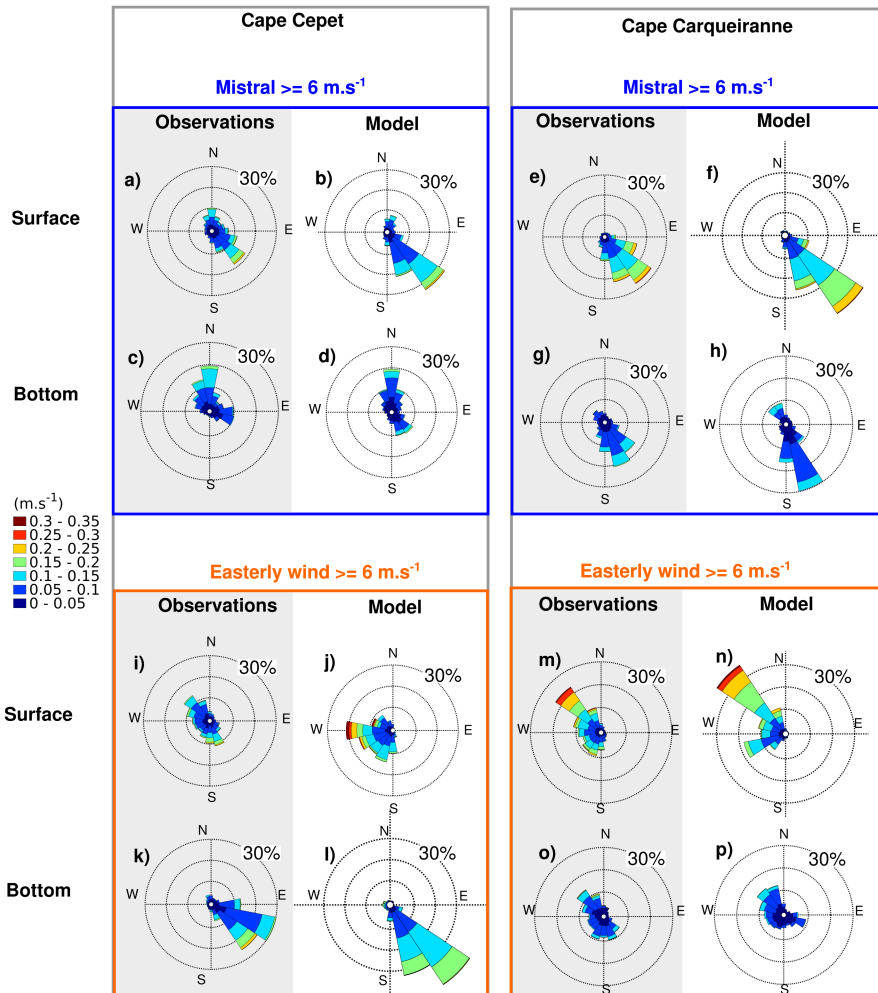


Figure 10: Current roses (m s<sup>-1</sup>) for ADACP observations and model output at location Cepet (left-hand side), and Carqueiranne (right-hand-side). Blue boxes (top) are for medium to strong Mistral conditions, orange boxes (bottom) for medium to strong easterly wind condition. For each box, observations (left) and model output (right) are represented for surface (top) and bottom (bottom) currents. Note current roses show the direction towards which the current flows.

( $0.35 \text{ m s}^{-1}$  versus  $0.20 \text{ m s}^{-1}$ ). At the bottom, current intensities and directions are overall the same, though observations show more variability in direction (Fig. 10c and d). For medium and strong easterly wind events (lower left box), differences appear between modelled and observed surface currents (Fig. 10i and j). While the observations show a north-westwards and south-southeastward flow with a maximum intensity of ca.  $0.20 \text{ m s}^{-1}$ , modelled currents flow towards the west to south-west at a significant higher velocity. At the bottom, currents have similar directions, flowing towards the south-east, with slightly more intense modelled currents (Fig. 10k and l). A possible explanation for the mismatches between the ADCP and model data (mostly situations in Fig. 10i and j), is the bathymetry approximation in the TBAY100 model, in particular near the capes, where the bathymetry is shallow and steep. We observe in the model outputs that current variability is very important near the Cape Cepet location and that this location is near the area where the current bypasses the LB in the model.

At Cap Carqueiranne, during medium and strong Mistral winds (upper right box), surface currents are stronger than at Cape Cepet and can reach up to  $0.25 \text{ m s}^{-1}$  during this period (Fig. 10e and f). Surface modelled and observed currents have similar directions and are flowing to the south-east out of the large bay. At the bottom, modelled and observed currents are weaker than at the surface (a maximum of ca.  $0.15 \text{ m s}^{-1}$ ) but they have almost the same directions, i.e. south-southeast for both model and observations (Fig. 10g and h). Accordingly, model and observations are very coherent at Cape Carqueiranne for Mistral conditions both in intensity and direction. During medium and strong easterly wind (lower right box), sur-

face currents flow north-westwards with a maximum intensity of  $0.3 \text{ m s}^{-1}$  for both model outputs and observations (Fig. 10m and n), which may correspond to an intrusion of offshore waters into the LB. Overall, the observed surface currents at the Cape Carqueiranne location seems to be more responsive to wind, as they appear to be stronger than at Cape Cepet, and are approximately downwind for both wind conditions. Finally, bottom currents during medium and strong easterly wind are weaker compared to the surface currents and have the same maximum intensity of  $0.15 \text{ m s}^{-1}$  for modelled data and observations. While the observed currents do not have a dominant direction, the modelled currents flow north-westwards and south-eastwards (Fig. 10o and p).

To summarize, the model results are coherent with most of the observed velocities direction at the ADCP locations. In terms of intensity, the model overestimates most of the time the occurrence and the intensity. The most important discrepancies appear at the western side of the LB boundary, at Cape Cepet, during easterly wind regimes, in particular at the surface. However the current rose of the ADCP (Fig. 10i) and of the model, do not show clear dominant currents, indicating that the circulation is very variable in this particular location. This variability is confirmed by the model results suggesting (Fig3a & 8b) that for the anticyclonic circulation, offshore waters may enter or not into the LB, leading to a different response at the ADCP location. Moreover we should recall that the ADCP experiment lasted 4 months in 2012 and the model simulation from February 2016 to April 2017. Interannual and seasonal variability could also explain part of the discrepancies.

If we compare the schematic circulations suggested by the model outputs and presented in the previous sections, during mistral regime the results are very coherent with both the BLP and the ACP. During easterly wind regime, the NIP appear at the bottom but not clearly at the surface. More ADCP moorings would be necessary to validate this circulation suggested by the simulations.

In conclusion, several factors influence the hydrodynamics of the Toulon Bay: the preceding conditions, offshore waters intrusions, wind intensity and direction. The important impact of wind on hydrodynamics within small semi-enclosed bays, was also observed in the Gulf of Fos, where wind events have a stronger influence on hydrodynamics than the shelf offshore current (Ulses et al., 2005). Even in small basins under strong tidal influence, wind events may interfere on local circulation, such as in Southern Australia (Black et al., 1993). The circulation patterns identified in this section highlight the possible export paths for contaminants which are discussed in the next section.

#### **4. Contaminant distribution**

Now that the circulation has been validated, the second objective is to better understand the distribution of contaminant in the area.

Chemical analysis of surface seawater samples from the Toulon Bay, obtained within the projects METFLUX, PREVENT and the MERMEX program by N. Layglon (MIO, University of Toulon) following an established method (Jean et al., 2012), have revealed the presence of elevated copper concentrations in March 2017, varying from 3 nM in the LB to 113 nM in

the SB (Fig. 11). While the distribution of dissolved copper is relatively uniform in LB (and close to background concentrations for the Mediterranean Sea, 1.6 nM; (Tovar-Sanchez et al., 2014)), steep concentration gradients were observed in the SB with maximum values measured in the docks of the civil (113 nM) and navy (67 nM) ports of Toulon and in the civil ports of La Seyne-sur-Mer (40 nM) and Saint-Mandrier (82 nM). This is in agreement with previous observations (e.g. Coclet et al., 2018), hence these ports can be considered as point sources of dissolved copper to the bay. Common sources of copper in harbours are antifouling paints which are applied to the hulls of boats to prevent growth of fouling organisms (e.g. Schiff et al., 2007). Since the ban of triorganotin formulations, most modern marine antifouling paints contain a Cu-based biocidal pigment (Turner, 2010) which has led to increased levels of dissolved copper in coastal waters, especially in and near ports (e.g. Biggs and D’Anna, 2012; Warnken et al., 2004). Accordingly, antifouling paints are hypothesised to be a major source of dissolved copper to the Toulon Bay.

To understand and evaluate the impact of the elevated levels of dissolved copper on the water quality of the Toulon Bay, distribution patterns were modelled under the influence of different wind conditions and seasonal variability was assessed via a 14-month simulation. Copper has been shown to have a high affinity for organic matter in the marine environment, forming dissolved organic copper species (e.g. Buck et al., 2007). Its distribution can thus be modelled as a passive tracer. Based on the surface distribution map of dissolved copper (Fig.11), copper was released as a passive tracer at three sources in the TBAY100 model: the civil ports of (1) Toulon, (2) la Seyne-

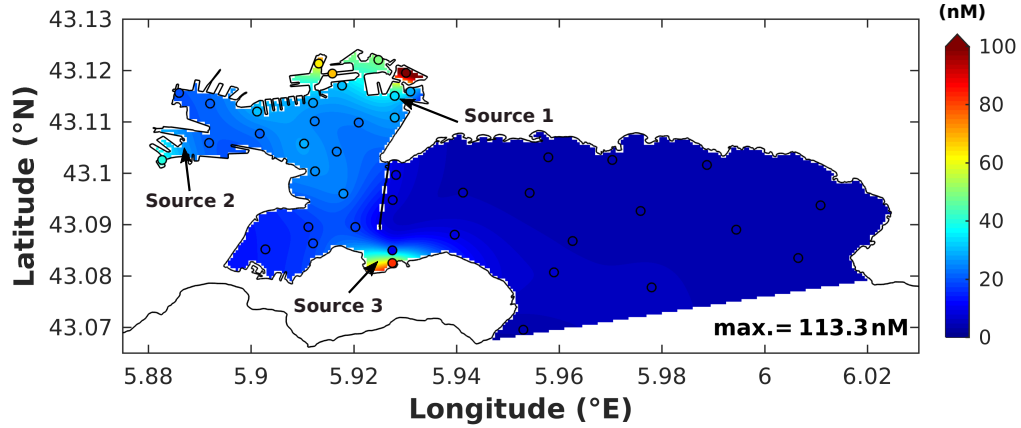


Figure 11: Sea surface distribution of copper (nM) measured on 20 March 2017 (av. wind speed and direction:  $2.4 \text{ m}^{-1}$  SE). Positions of the three contaminant sources in the TBAY100 model: Toulon civil port (source 1), la Seyne-sur-Mer civil port (source 2), and Saint-Mandrier civil port (source 3).

sur-Mer and (3) Saint-Mandrier (see Fig. 1B for the precise location in the TBAY100 model). As the majority of the berths in the ports are occupied year-round, copper leaching from anti-fouling paints is considered to be a constant process and was therefore modelled as a continuous source. The quantity of copper released per time step at each source ( $Cu_{\text{source}}$ ; nmol  $\text{dt}^{-1}$ ) was calculated based on the capacity of each port (i.e. number of berths) using the following equation:

$$Cu_{\text{source}} = N_{\text{berths}} \times S_{\text{mean}} \times AR \times dt \quad (2)$$

where  $N_{\text{berths}}$  is the number of berths per port,  $S$  is the standard estimate for wetted hull surface area (i.e.  $41 \text{ m}^2$ ) of a typical recreational boat (12 m long with a beam of 4 m) used by paint manufacturers (i.e. the length

by the beam width by 0.85, a standard conversion factor; Earley et al. (2014) ) and  $AR$  is an average release rate of antifouling paint ( $6.9 \text{ nmol m}^{-2} \text{ s}^{-1}$ ). The latter is based on estimates for cumulative passive copper leaching (i.e. without considering cleaning activities and boat usage) during a typical paint life cycle of three years for 2 types of paint ( $4164 \text{ ug cm}^{-2}$  or  $1388 \text{ ug cm}^{-2} \text{ yr}^{-1}$  which corresponds to  $6.9 \text{ nmol m}^{-2} \text{ s}^{-1}$ ), which was derived from in situ measurements in San Diego Bay (Earley et al., 2014). Accordingly,  $AR$  provides a minimum baseline for leaching rates of Cu from antifouling paints into the marine environment.

Table 2: Estimates of copper release rates at the three identified point sources in Toulon Bay.  $N_{berths}$  is the number of berths per port, and Cu is the quantity of copper released per time step (nmol/5s)

	$N_{berths}$	Cu (nmol/5s)
Source 1 (Toulon civil port)	982	$1.5 \times 10^6$
Source 2 (la Seyne-sur-Mer)	300	$4.5 \times 10^5$
Source 3 (Saint-Mandrier)	800	$1 \times 10^6$

#### 4.0.1. Wind dependent contaminant distribution patterns

As shown in section 3.3 several circulation patterns could be correlated with two main wind directions: the Mistral and the easterly wind. The circulation patterns were depending on the wind intensity and direction for the former and the existence of offshore waters intrusions for the latter. The influence of these four circulation patterns on the dispersion of dissolved contaminants in the Toulon Bay was examined by running idealized simulations,

imposing a constant wind during 2 days instead of using the ARPEGE atmospheric model as external wind forcings. Care was taken to select two days with wind conditions similar to the imposed one, to avoid too important numerical instabilities, and a possible model blow-up. The same patterns were obtained for multiple dates for each of the four wind case scenarii and associated circulation patterns: 1) Mistral  $8 \text{ m s}^{-1}$  (ACP), 2) Mistral  $16 \text{ m s}^{-1}$  (BLP), 3) easterly wind with offshore waters intrusion (IP) and 4) easterly wind without offshore waters intrusion (NIP), underlining the representativeness of these contaminant distribution patterns for each scenario.

At medium wind intensity ( $8 \text{ m s}^{-1}$ ), the plume of dissolved contaminants released in the SB spreads into almost the entire LB (Fig. 12-A1). Overall concentration maxima occur at the surface in the entire bay with exception of a small eddy, which is formed at the exit of the SB. This contaminant plume is originated from source 2 and 3 that are evacuated from the SB during the time span of 2 days. The waters exiting the SB encounter an incoming vein flowing westward into the LB and mix because of this front preventing them from spreading in the whole LB. The SB waters bypass this front by following an anticyclonic motion into the LB, spreading the contaminant at the surface of the LB (Fig. 12-A2). The dispersion of the contaminants released at the Toulon civil port (source 1) remains confined to the northeast sector of the SB. Mistral winds of high intensity ( $16 \text{ m s}^{-1}$ ) export dissolved contaminants to the LB and beyond, until the Giens peninsula, in 2 days time (Fig. 12-B1) demonstrating the wind-driven circulation in the Toulon Bay area. The majority of the contaminants remain at the surface (Fig. 12-B2).

In the case of easterly winds, simulations have demonstrated that the

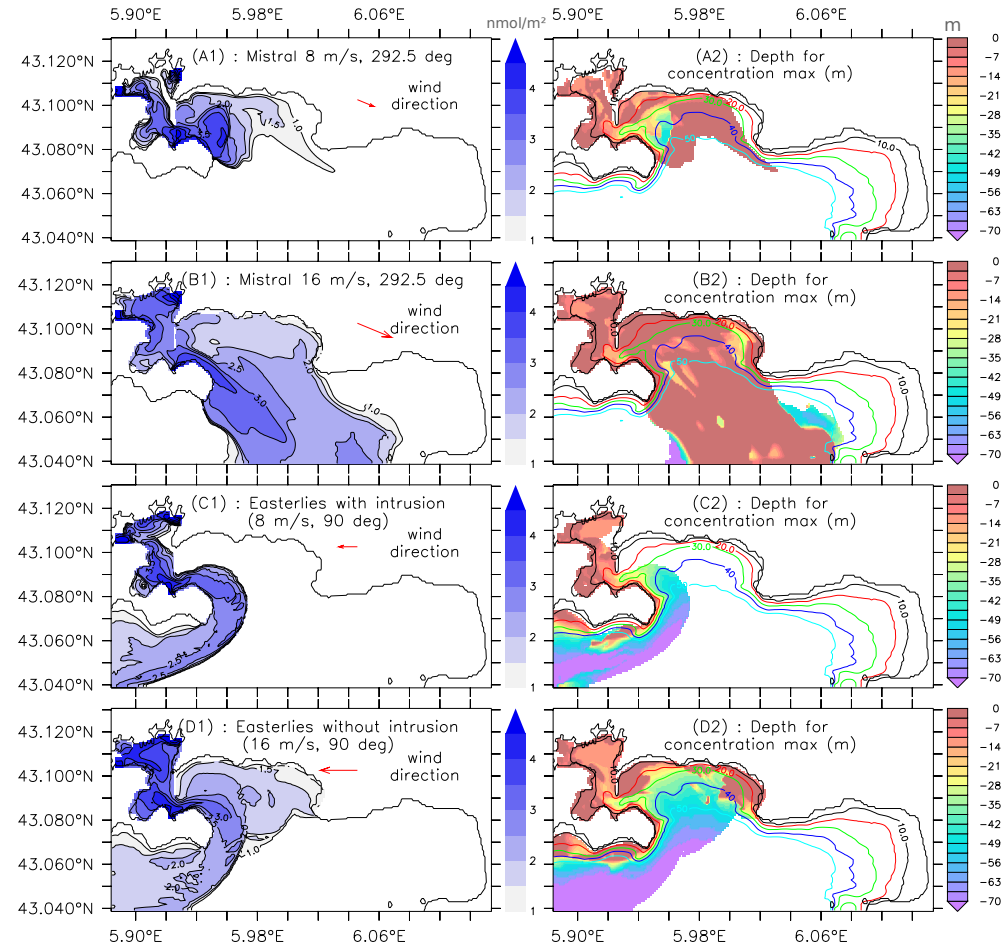


Figure 12: On the left (A1, B1, C1, D1), test cases of contaminant release for the 3 sources source 1, source 2, source 3. Integration of tracers on the whole column water, logarithmic scale ( $\text{nmol m}^{-2}$ ). On the right (A2, B2, C2, D2), depth where the tracer concentration is the maximum (m). Different circulations with constant wind conditions are simulated: ACP with medium mistral (A), BLP with strong mistral (B), IP (offshore waters intrusion into the LB) with medium easterly wind (C) and NIP (without intrusion) with strong easterly wind (D).

presence or absence of offshore waters intrusions is the determining factor defining the contaminant distribution patterns. It is correlated with wind characteristics (intensity and direction), so that a medium SE wind induces an entrance of offshore waters into the LB whereas a strong NE wind tends to prevent an intrusion of waters into the LB. During easterly wind conditions with an intrusion into the LB (corresponding to the intrusion pattern and a wind of medium intensity), the contaminant plume is exiting the Toulon Bay at depth along a narrow route around the Saint-Mandrier peninsula (Fig. 12-C1), following the bathymetry. Passed this cape, pollutants resurface on the south coast of the peninsula while remaining at mid-water depths further offshore. Once at this point, pollutants are likely taken up in the NC and quickly exported westwards along the coast. Without offshore waters intrusions in the LB, with a strong easterly wind, contaminants are distributed over the entire LB and are evacuated following the passageway along the Saint-Mandrier peninsula (Fig. 12-D1). While the dissolved contaminants remain on the surface, in the SB they sink to the bottom once passed the seawall. Passing the peninsula, the contaminant plume mainly follows the bathymetry.

In conclusion, the model shows that, outside of the Toulon Bay, especially the south coast of the Saint-Mandrier peninsula is directly subjected to frequent plumes of dissolved contaminants (for 2 out of 4 scenarii, which corresponds to medium and strong easterly wind periods or 9% of the total time). As the contaminants show a tendency of staying in surface layers, extra vigilance may be required for the quality of surface waters in this area. Furthermore, dissolved contaminants, originating from Toulon Bay,

may reach the Marine National Park of Port-Cros, under mainly strong Mistral winds driving a bi-layer circulation pattern which is estimated to occur ca. 20% of the time, given that medium to strong Mistral correspond to 24.9% of the total time. Accordingly, the impact of Toulon Bay's contaminated waters on the National Park appears possible, which warrants further investigation using a model with a domain that extends to the National Park.

#### *4.0.2. Seasonal variability of contaminant dispersion*

A 14-month simulation was conducted to assess the seasonal variability of dissolved contaminant distributions in the Toulon Bay. Therefore the Cu distribution map in Fig. 11 (based on 42 observations) was used as initial condition and copper was released at a continuous rate (Table 2) from the three point sources. The main interest of this simulation is to evaluate the potential impact of contaminant release on surface waters (top 5 m of the water column) in recreational zones such as near beaches and in areas exploited for aquaculture, where water quality may impact public health. Accordingly, Fig. 13 shows the temporal variation in dissolved copper at the highly frequented beaches of Mourillon (Large Bay), the aquaculture site Lazaret (Small Bay) and, for comparison, the northern SB close to sources 1 and 2 (Fig.1B). The model results show that at the three locations, the surface waters are more concentrated in dissolved copper (up to 5 times the background signal) during spring and early summer. This may be due to the fact that this period is generally characterized by winds with a lower intensity (Fig. 13), which implies weaker surface currents and longer residence time (Dufresne et al., 2014). As dissolved contaminant dispersion is wind-driven in the SB, the dispersion of dissolved copper is reduced and an accumulation can

be observed in the entire SB. On the other hand, medium Mistral wind (6-10  $\text{m s}^{-1}$ ) with an anticyclonic pattern (Fig. 9b), is probably responsible for the observed elevated copper concentrations in the waters of Mourillon (Fig. 12-A2). Accordingly, the observed pattern of a degraded water quality in spring-summer in the Toulon Bay, merits to be tested in the future with observations to validate the coupled hydrodynamic and passive tracer model as a useful tool for pollution management. The low dissolved copper concentrations in winter, are mostly likely due to the stronger wind intensities ( $> 15 \text{ m s}^{-1}$ ) and the frequent alternation between Mistral and easterly winds promoting water exchanges between SB and LB as demonstrated by [Dufresne et al. \(2014\)](#).

The 1-year simulation is not sufficient for the contaminant continuously released at the source points to impact the far east side of the bay. Therefore, the temporal variability of contaminant dispersion will not be discussed for the beaches located at the far east side of the TBAY model domain.

Nonetheless, copper concentrations in these areas remain close to background values for the Mediterranean Sea (i.e. 1.6 nM; [Tovar-Sanchez et al. \(2014\)](#)) after one year. Although seasonal variability was the focus of the 14-month simulation, a validation of the tracer model was performed, comparing the Cu concentration map with the model output for the same day, 20 March 2017. This comparison shows that the surface Cu concentrations are underestimated compared to the measured values (Fig. S1 and S2 in Supplementary Material), while the concentration gradient across the Toulon Bay is reproduced. The estimates are especially low in the small bay which is most likely due to the minimum Cu leaching rates used in the model (section

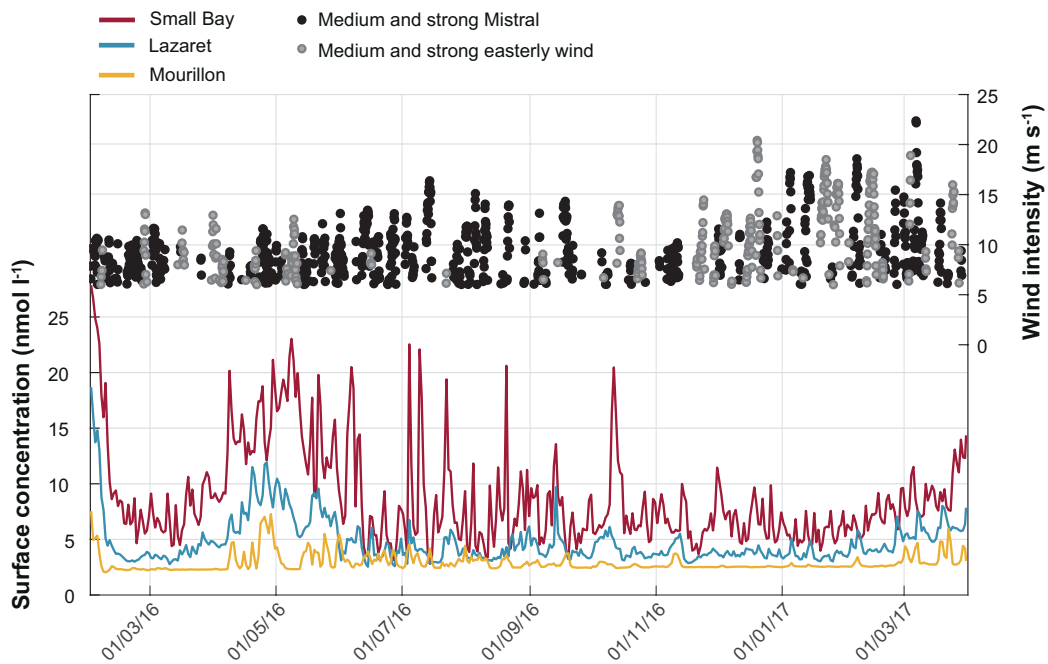


Figure 13: Surface distribution of Copper (nmol l<sup>-1</sup>) during a 14 months simulation with the model TBAY100, in three studied sites, corresponding to the boxes Fig. 1. Wind intensity (m s<sup>-1</sup>) for medium and strong wind events: black dots for Mistral events, grey dots for easterly wind events.

4). The latter do not take into account boat cleaning activities and boat traffic, two activities that are particularly concentrated in the small bay (but difficult to quantify) and are known to have an impact on Cu leaching from antifouling paints. Accordingly more efforts are needed in quantifying Cu leaching rates to improve copper distribution modelling studies in coastal areas, where antifouling paints are likely a major source of Cu.

## 5. Conclusions with discussion

The aim of this study was to investigate circulation patterns and scenarios of contaminant dispersion depending on weather conditions, thanks to the very high resolution configuration TBAY100 (configuration set up with the MITgcm ocean model). As previous studies focused on the exchange between SB and LB, this study focused on the circulation occurring in the LB and the exchanges with offshore waters, to assess the potential impact of the heavily contaminated waters of Toulon Bay on the surrounding environment, including the Marine Port-Cros National Park.

Model simulations have highlighted that the circulation in Toulon Bay is mainly wind-driven. However, offshore waters intrusions do occur and can induce strong currents inside the bay. These intrusions may be NC intrusions as in the Hyeres Bay upstream and an assessment of this hypothesis would be part of a future work. The tides contribute only for 3-4 cm on average of the free surface elevation, with a maximum of 20 cm in our zone, as confirmed by local observations (Rey et al., 2019). Therefore, we can say that the tide has a minor impact compared to other forcings. Overall, four circulation patterns could be identified. Medium to strong Mistral events do most frequently (81

%) generate a Bi-layer pattern and less often (13 %) an Anticyclonic pattern. In both patterns, the plume of dissolved contaminants spreads at the surface over the entire LB, but in summer period, the contaminant plume flows towards the Giens peninsula. The anticyclonic circulation appears mostly during winter periods suggesting that the absence of stratification can play a role for its occurrence. The impact of stratification on this schematic circulation will be addressed in a future work. When the wind episode is long enough and considering the frequent occurrence of the Bi-layer pattern, there could be exchanges of contaminants with the Hyeres Bay and the Port-Cros National Park. Medium to strong easterly winds induce offshore waters intrusions into the LB (78 %) associated with a cyclonic circulation (Intrusion Pattern). Under these conditions, contaminants are spreading into a narrow vein above the bottom, flowing around Saint-Mandrier peninsula before probably meeting the NC offshore. At the same time, it can also spread inside the LB before being carried offshore Saint-Mandrier peninsula if there is no offshore waters intrusion into the LB (Non Intrusion Pattern).

In addition, medium to strong Mistral events typically create upwelling events in the north-western Mediterranean. These events also occur downstream in the Gulf of Lion (Millot, 1979; Barrier et al., 2016) and the Bay of Marseille (Pairaud et al., 2011). They are known to strongly impact the biogeochemistry of surrounding waters (Ross et al., 2016). To our knowledge, there is no evidence in the scientific literature for these upwellings in the area near Toulon, but recent observational data is confirming such phenomena (Rey et al., 2019). Some upwelling episodes could be identified in our simulations, but a specific study on these phenomena will have to be carried

out, focusing on vertical movements, at very short time and space scale.

As to optimise predictions of contaminant distribution in this exceptionally polluted area, an increment and adjustment of locations of moored ADCP locations is envisaged in the near future, as well as an assessment of non hydrostatic effects on the circulation in Toulon Bay. Moreover, other suggestions for future work are: evaluating the dispersion of contaminants toward the Marine National Park Port-Cros using a model domain incorporating the park and implementing a sedimentary package into the model as to model also dispersion patterns for contaminants with a high particle affinity such as lead.

## **6. Acknowledgements**

This work was granted access to the HPC resources of Aix-Marseille Université financed by the project Equip@Meso (ANR-10-EQPX-29-01) of the program “Investissements d’Avenir” supervised by the Agence Nationale de la Recherche. The TBAY100 simulations were also performed using GENCI-IDRIS (Grant A0030101707). Mazoyer C. PhD grants is supported by the French Ministry of Research. This work was supported by the EU-funded Project IMPACT (PC IFM 2014-2020, Prot. ISMAR n. 0002269). The authors would like to thank Céline Duffa at IRSN (Institut de Radioprotection et de Sûreté Nucléaire) for kindly providing ADCP data. We would like to thank Nicolas Layglon for providing the copper concentration results which were obtained during his Master 2 training at MIO (University of Toulon) as part of the METFLUX and PREVENT projects and the MERMEX program. We also thank the SHOM for providing the bathymetry of the Toulon

Bay. We dedicated this study to our colleague and friend Dr. Cédric Garnier.

## References

- Alberola, C., Millot, C., 2003. Circulation in the French mediterranean coastal zone near Marseilles: the influence of wind and the Northern Current. *Continental Shelf Research* 23, 587–610, IU.
- Alberola, C., Millot, C., Font, J., Jan. 1995a. On the seasonal and mesoscale variabilities of the Northern Current during the PRIMO-0 experiment in the western Mediterranean-sea. *Oceanologica Acta* 18 (2), 163–192.
- Alberola, C., Millot, C., Font, J., Jan. 1995b. On the seasonal and mesoscale variabilities of the Northern Current during the PRIMO-0 experiment in the western Mediterranean-sea. *Oceanologica Acta* 18 (2), 163–192.
- Auclair, F., Marsaleix, P., Estournel, C., 2001. The penetration of the Northern Current over the Gulf of Lions (Mediterranean) as a downscaling problem. *Oceanologica Acta* 24 (6), 529–544.
- Barrier, N., Petrenko, A. A., Ourmières, Y., Mar. 2016. Strong intrusions of the Northern Mediterranean Current on the eastern Gulf of Lion: insights from in-situ observations and high resolution numerical modelling. *Ocean Dynamics* 66 (3), 313–327.
- Bethoux, J. P., Prieur, L., Nyffeler, F., Jan. 1982. The Water Circulation in the North-Western Mediterranean Sea, its Relations with Wind and Atmospheric Pressure. In: Nihoul, J. C. J. (Ed.), Elsevier Oceanography Series. Vol. 34 of Hydrodynamics of Semi-Enclosed Seas. Elsevier, pp. 129–142.

- Biggs, T. W., D'Anna, H., Mar. 2012. Rapid increase in copper concentrations in a new marina, San Diego Bay. *Marine Pollution Bulletin* 64 (3), 627–635.
- Black, K., Hatton, D., Rosenberg, M., 1993. Locally and Externally-Driven Dynamics of a Large Semi-Enclosed Bay in Southern Australia. *Journal of Coastal Research* 9 (2), 509–538.
- Buck, K. N., Ross, J. R. M., Russell Flegal, A., Bruland, K. W., Sep. 2007. A review of total dissolved copper and its chemical speciation in San Francisco Bay, California. *Environmental Research* 105 (1), 5–19.
- Coclet, C., Garnier, C., Delpy, F., Jamet, D., Durrieu, G., Le Poupon, C., Mayer, M., Misson, B., Apr. 2018. Trace metal contamination as a toxic and structuring factor impacting ultraphytoplankton communities in a multicontaminated Mediterranean coastal area. *Progress in Oceanography* 163, 196–213.
- Conan, P., Millot, C., Jan. 1995. Variability of the northern current off Marseilles, western Mediterranean-sea, from February to June 1992. *Oceanologica Acta* 18 (2), 193–205.
- Csanady, G. T., Oct. 1973. Wind-Induced Barotropic Motions in Long Lakes. *Journal of Physical Oceanography* 3 (4), 429–438.
- Dang, D. H., Schäfer, J., Brach-Papa, C., Lenoble, V., Durrieu, G., Dutruch, L., Chiffoleau, J.-F., Gonzalez, J.-L., Blanc, G., Mullot, J.-U., Mounier, S., Garnier, C., Oct. 2015. Evidencing the Impact of Coastal Contaminated Sediments on Mussels Through Pb Stable Isotopes Composition. *Environmental Science & Technology* 49 (19), 11438–11448.
- Declerck, A., Ourmières, Y., Molcard, A., Nov. 2016. Assessment of the coastal

- dynamics in a nested zoom and feedback on the boundary current: the North-Western Mediterranean Sea case. *Ocean Dynamics* 66 (11), 1529–1542.
- Duffa, C., Dufois, F., Coudray, S., Nov. 2011. An operational model to simulate post-accidental radionuclide transfers in Toulon marine area: preliminary development. *Ocean Dynamics* 61 (11), 1811–1821.
- Dufresne, C., Duffa, C., Rey, V., 2014. Wind-forced circulation model and water exchanges through the channel in the Bay of Toulon. *Ocean Dynamics* 64 (2), 209–224.
- Dufresne, C., Duffa, C., Rey, V., Verney, R., Mar. 2018. Hydro-sedimentary model as a post-accidental management tool: Application to radionuclide marine dispersion in the Bay of Toulon (France). *Ocean & Coastal Management* 153, 176–192.
- Earley, P. J., Swope, B. L., Barbeau, K., Bundy, R., McDonald, J. A., Rivera-Duarte, I., Jan. 2014. Life cycle contributions of copper from vessel painting and maintenance activities. *Biofouling* 30 (1), 51–68.
- Fiandrino, A., Ouisse, V., Dumas, F., Lagarde, F., Pete, R., Malet, N., Le Noc, S., de Wit, R., Jun. 2017. Spatial patterns in coastal lagoons related to the hydrodynamics of seawater intrusion. *Marine Pollution Bulletin* 119 (1), 132–144.
- Flexas, M. M., Durrieu de Madron, X., Garcia, M. A., Canals, M., Arnau, P., Jun. 2002. Flow variability in the Gulf of Lions during the MATER HFF experiment (March–May 1997). *Journal of Marine Systems* 33-34, 197–214.
- Guihou, K., Marmain, J., Ourmières, Y., Molcard, A., Zakardjian, B., Forget, P., Jun. 2013. A case study of the mesoscale dynamics in the North-Western

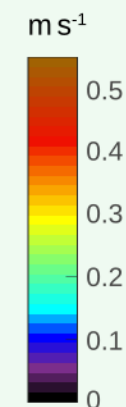
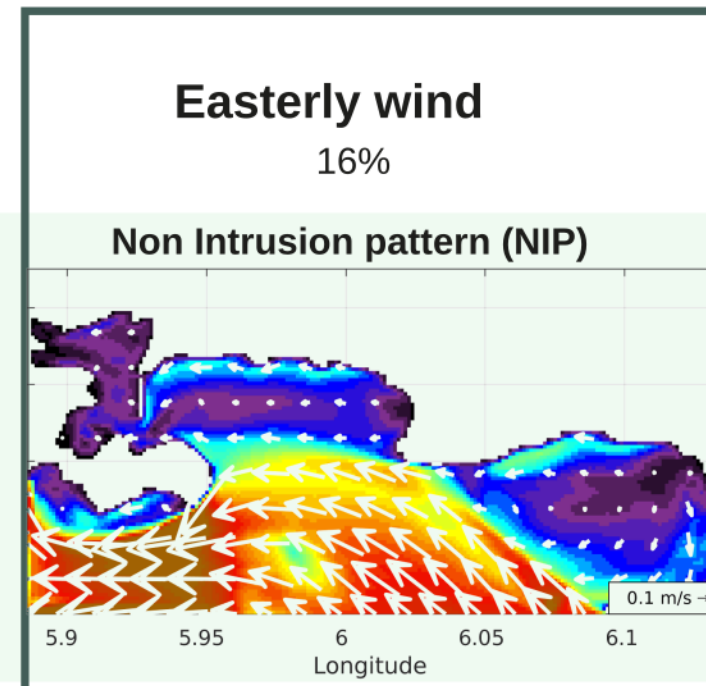
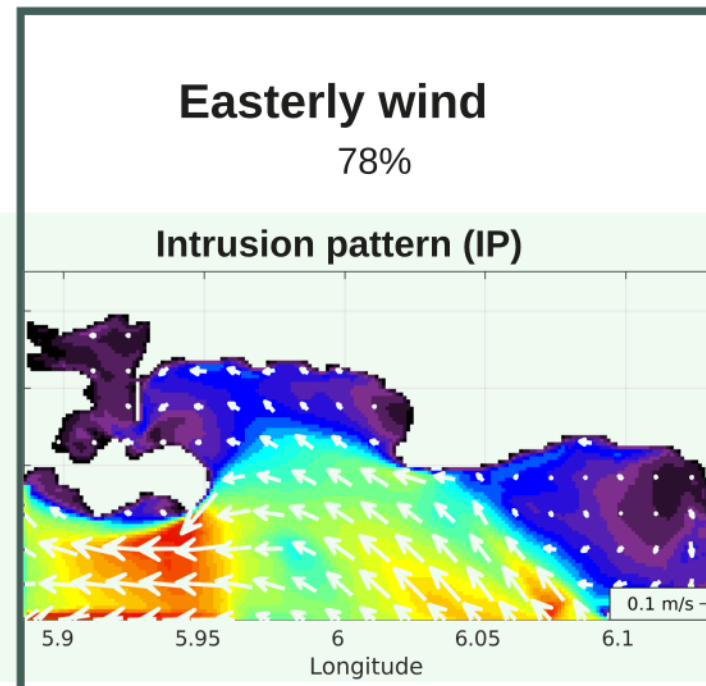
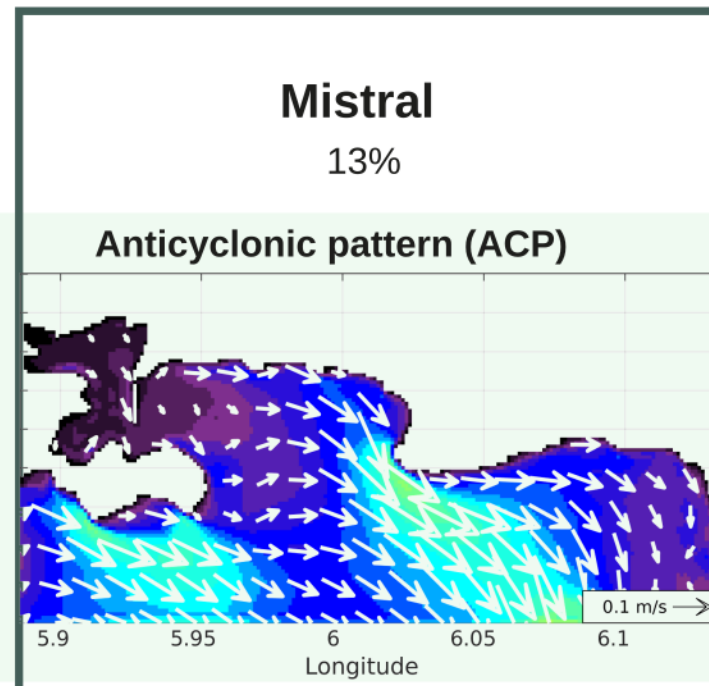
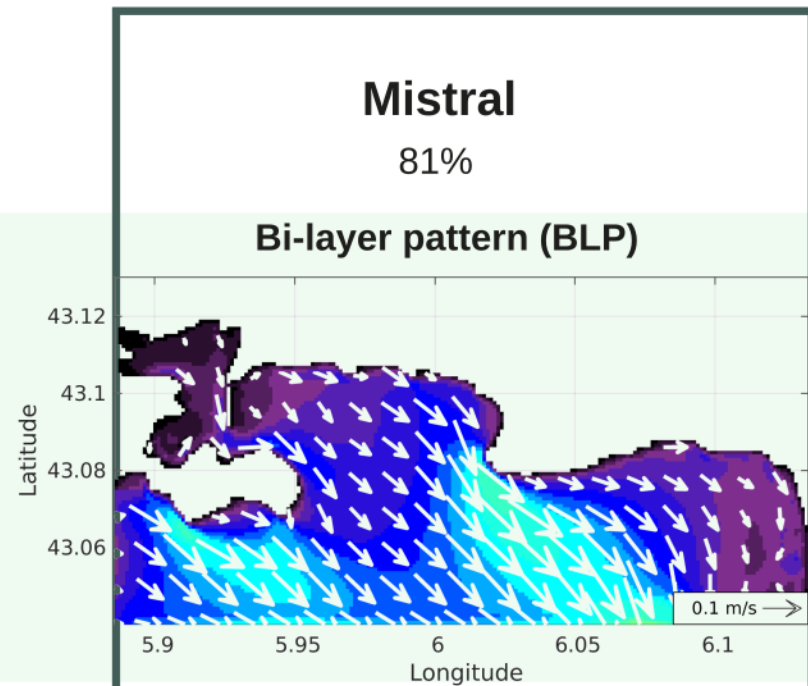
- Mediterranean Sea: a combined data–model approach. *Ocean Dynamics* 63 (7), 793–808.
- Jean, N., Dumont, E., Durrieu, G., Balliau, T., Jamet, J.-L., Personnic, S., Garnier, C., Sep. 2012. Protein expression from zooplankton communities in a metal contaminated NW mediterranean coastal ecosystem. *Marine Environmental Research* 80 (Supplement C), 12–26.
- Lapouyade, A., Durrieu de madron, X., May 2001. Seasonal variability of the advective transport of particulate matter and organic carbon in the Gulf of Lion (NW Mediterranean). *Oceanologica Acta* 24 (3), 295–312.
- Large, G., McWilliams, C., Doney, S., 1994. Oceanic vertical mixing: A review and a model with a nonlocal boundary-layer parameterization. *Reviews of Geophysics* 32 (4), 363–403.
- Large, G., Yeager, S., 2004. Diurnal to decadal global forcing for ocean and sea-ice models: The data sets and flux climatologies.
- Leith, C. E., Mar. 1968. Diffusion Approximation for Two-Dimensional Turbulence. *The Physics of Fluids* 11 (3), 671–672.
- Leith, C. E., Nov. 1996. Stochastic models of chaotic systems. *Physica D: Nonlinear Phenomena* 98 (2), 481–491.
- Limeburner, R., Lrish, J. D., Brown, W. S., Halliwell, G. R., Allen, J. S., Winant, C. D., Send, E., Lentz, S. J., Rosenfeld, L. K., Beardsley, R. C., et al., 1985. CODE-2: Moored array and large-scale data report. Woods Hole Oceanographic Institution.

- Malačić, V., Petelin, B., Vodopivec, M., 2012. Topographic control of wind-driven circulation in the northern Adriatic. *Journal of Geophysical Research: Oceans* 117 (C6).
- Marshall, J., Adcroft, A., Hill, C., Perelman, L., Heisey, C., Mar. 1997. A finite-volume, incompressible Navier Stokes model for studies of the ocean on parallel computers. *Journal of Geophysical Research: Oceans* 102 (C3), 5753–5766.
- Millot, C., Jan. 1979. Wind induced upwellings in the gulf of lions. *Oceanologica Acta* 2 (3), 261–274.
- Millot, C., Broyard, R., Metais, O., Tine, J., Jan. 1981. Les oscillations propres de la rade de Toulon. *Oceanologica Acta* 4 (3), 259–262.
- Ourmières, Y., Zakardjian, B., Béranger, K., Langlais, C., 2011. Assessment of a NEMO-based downscaling experiment for the North-Western Mediterranean region: Impacts on the Northern Current and comparison with ADCP data and altimetry products. *Ocean Modelling* 39 (3–4), 386–404.
- Pairaud, I. L., Gatti, J., Bensoussan, N., Verney, R., Garreau, P., Oct. 2011. Hydrology and circulation in a coastal area off Marseille: Validation of a nested 3d model with observations. *Journal of Marine Systems* 88 (1), 20–33.
- Petrenko, A., Sep. 2003. Variability of circulation features in the Gulf of Lion NW Mediterranean Sea. Importance of inertial currents. *Oceanologica Acta* 26 (4), 323–338.
- Pouget, F., Schäfer, J., Dutruch, L., Garnier, C., Tessier, E., Dang, D. H., Lancelot, L., Mullot, J.-U., Lenoble, V., Blanc, G., May 2014. Sources and historical record of tin and butyl-tin species in a Mediterranean bay (Toulon Bay, France). *Environmental Science and Pollution Research* 21 (10), 6640–6651.

- Rey, V., Dufresne, C., Fuda, J., Mallarino, D., Missamou, T., Paugam, C., Rougier, G., Taupier-Letage, I., 2019. On the use of long term observation of water level and temperature along the shore for a better understanding of the dynamics: Example of Toulon area, France. Under review.
- Ross, O. N., Fraysse, M., Pinazo, C., Pairaud, I., Mar. 2016. Impact of an intrusion by the Northern Current on the biogeochemistry in the eastern Gulf of Lion, NW Mediterranean. *Estuarine, Coastal and Shelf Science* 170.
- Rubio, A., Taillandier, V., Garreau, P., Nov. 2009. Reconstruction of the Mediterranean northern current variability and associated cross-shelf transport in the Gulf of Lions from satellite-tracked drifters and model outputs. *Journal of Marine Systems* 78, S63–S78.
- Sammari, C., Millot, C., Prieur, L., Jun. 1995. Aspects of the seasonal and mesoscale variabilities of the Northern Current in the western Mediterranean Sea inferred from the PROLIG-2 and PROS-6 experiments. *Deep Sea Research Part I: Oceanographic Research Papers* 42 (6), 893–917.
- Schiff, K., Brown, J., Diehl, D., Greenstein, D., Mar. 2007. Extent and magnitude of copper contamination in marinas of the San Diego region, California, USA. *Marine Pollution Bulletin* 54 (3), 322–328.
- Schoen, J. H., Stretch, D. D., Tirok, K., Jun. 2014. Wind-driven circulation patterns in a shallow estuarine lake: St Lucia, South Africa. *Estuarine, Coastal and Shelf Science* 146, 49–59.
- Taupier-Letage, I., Millot, C., Apr. 1986. General hydrodynamical features in the ligurian sea inferred from the dyome experiment. *Oceanologica Acta* 9 (2), 119–131.

- Tessier, E., Garnier, C., Mullot, J.-U., Lenoble, V., Arnaud, M., Raynaud, M., Mounier, S., Oct. 2011. Study of the spatial and historical distribution of sediment inorganic contamination in the Toulon bay (France). *Marine Pollution Bulletin* 62 (10), 2075–2086.
- Tine, 1981. *Hydrodynamisme en Rade Abri de Toulon*.
- Tovar-Sanchez, A., Arrieta, J. M., Duarte, C. M., Sanudo-Wilhelmy, S. A., 2014. Spatial gradients in trace metal concentrations in the surface microlayer of the Mediterranean Sea. *Frontiers in Marine Science* 1.
- Turner, A., Feb. 2010. Marine pollution from antifouling paint particles. *Marine Pollution Bulletin* 60 (2), 159–171.
- Ulses, C., Grenz, C., Marsaleix, P., Schaaff, E., Estournel, C., Meulé, S., Pinazo, C., May 2005. Circulation in a semi-enclosed bay under influence of strong freshwater input. *Journal of Marine Systems* 56 (1), 113–132.
- Warnken, J., Dunn, R. J. K., Teasdale, P. R., Nov. 2004. Investigation of recreational boats as a source of copper at anchorage sites using time-integrated diffusive gradients in thin film and sediment measurements. *Marine Pollution Bulletin* 49 (9), 833–843.

Hydrodynamic  
circulation



Contaminant  
dispersion



copper from  
antifouling paints

